Published in final edited form as:
Ultrasound Med Biol. 2013 May ; 39(5): 813–824. doi:10.1016/j.ultrasmedbio.2012.12.008.

Clot retraction affects the extent of ultrasound-enhanced thrombolysis in an *ex vivo* porcine thrombosis model

Jonathan T. Sutton[1], **Nikolas M. Ivancevich, Ph.D.**[2,3], **Stephen R. Perrin Jr., M.S**[1], **Deborah C. Vela, M.D., M.S.**[4], and **Christy K. Holland, Ph.D.**[1,2]

[1]University of Cincinnati; Biomedical Engineering Program, College of Engineering and Applied Science; Cincinnati, OH USA

[2]University of Cincinnati; Internal Medicine, Division of Cardiovascular Diseases; Cincinnati, OH USA

[3]Siemens Medical Solutions; Issaquah, WA USA

[4]Texas Heart Institute, Cardiovascular Pathology; Houston, TX USA

Abstract

Using an FDA-approved contrast agent (Definity®) and thrombolytic drug (rt-PA), we investigated ultrasound-enhanced thrombolysis in two whole-blood clot models. Porcine venous blood was collected from donor hogs and coagulated in two different materials. This method produced clots with differing compositional properties, as determined by routine scanning electron microscopy and histology. Clots were deployed in an ex vivo porcine thrombolysis model, while an intermittent ultrasound scheme previously developed to maximize stable cavitation was applied and acoustic emissions were detected. Exposure of clots to 3.15 μg/mL rt-PA promoted lysis in both clot models, compared to exposure to plasma alone. However, in the presence of rt-PA, Definity®, and ultrasound, only unretracted clots experienced significant enhancement of thrombolysis compared to treatment with rt-PA. In these clots, microscopy studies revealed loose erythrocyte aggregates, a significantly less extensive fibrin network, and a higher porosity, which may facilitate increase penetration of thrombolytics by cavitation.

Keywords

thrombolysis; clot retraction; ultrasound; stable cavitation; inertial cavitation; drug delivery

Introduction

Ischemic Stroke

Ischemic stroke is a deadly and debilitating condition that imposes a significant financial burden on health care systems worldwide. Internationally in 2008, 17.2% of all noncommunicable disease deaths were attributed to stroke. Two percent of all health care costs in the United States are attributed to the direct and indirect costs of stroke (Goldstein et

Corresponding Author: Jonathan T. Sutton, University of Cincinnati, 231 Albert Sabin Way, Cardiovascular Center Rm. 3940, Cincinnati, OH 45267, Work: 1 (513) 558 - 5505, Fax: 1 (513) 558 - 6102, suttonjt@mail.uc.edu.

al. 2009). The lack of oxygen transport to brain tissue during stroke can impair motor and cognitive functions permanently. While alternative therapies are currently under investigation (Alexandrov et al. 2010), intravenous (IV) administration of recombinant tissue-plasminogen activator (rt-PA) within 6 hours of symptom onset remains the only approved treatment for ischemic stroke (Hacke et al. 2008). In one clinical trial however, over 70% of patients receiving IV rt-PA did not recover completely after three months, most likely due to tissue damage prior to treatment or incomplete recanalization (Alexandrov et al. 2004).

Differential sensitivity to rt-PA thrombolysis may be explained by the variety of thrombi from a host of origins that dislodge and travel to the cerebral vasculature (Molina et al. 2005). Different thrombus subtypes are known to display unique qualities. For example, thrombi of cardioembolic origin—richer in erythrocyte content (Silvain et al. 2011)—are thought to be easiest to lyse with rt-PA, in contrast to fibrous thrombi from large vessel thrombotic disease (Molina et al. 2004). Other clot properties (Gersh et al. 2009), including fiber diameter (Gabriel et al. 1992), fiber orientation (Gersh et al. 2010), and clot age or degree of retraction (Kramer et al. 2008; Holland et al. 2008) also affect the lytic rates of clots *in vitro* and *in vivo*.

Retraction changes the internal structure and composition of a clot considerably (Kunitada et al. 1992) by purging the clot of its serum, resulting in volume reduction (Fox and Phillips 1983). Various experimental methods can be implemented to modify the degree of clot retraction. Cytochalasin D inhibits actin polymerization in platelet filopodia and affects thrombolytic efficacy (Kunitada et al. 1992). Alternatively, the different charge densities on surfaces used for *in vitro* clot formation activate platelets to varying degrees, affecting clot retraction (Faxalv et al. 2008). Retraction changes the internal fibrin architecture of a clot and reduces its permeability and the volume of the clot's fluid phase, including soluble plasminogen (Weisel 2007; Weisel and Litvinov 2008). By diminishing this important substrate, fluid loss from retraction limits the effectiveness of t-PA, weakening the body's natural thrombolytic mechanism during ischemic stroke.

Ultrasound-enhanced thrombolysis (UET) is an attractive adjuvant to conventional rt-PA therapy. Investigators (Blinc et al. 1994; Datta et al. 2008; Hitchcock et al. 2011) discuss a number of potential mechanisms of action, citing increased penetration of fibrinolytics into the clot (Blinc et al. 1994; Datta et al. 2008; Francis et al. 1995) and removal of fibrin degradation products by stable cavitation-induced microstreaming (Datta et al. 2008). When a microbubble oscillates persistently near the surface of a clot, local fluid convection caused by nonlinear oscillations could facilitate these mechanisms (Collis et al. 2010b). In a clinical trial of UET however, arterial recanalization and patient recovery increased marginally in the presence of ultrasound (US) and microbubbles, compared to rt-PA treatment (Molina et al. 2009).

Given the wealth of knowledge on clot susceptibility to rt-PA thrombolysis and the wide array of *in vivo* thrombus characteristics, we aimed to investigate the dependence of ultrasound-enhanced thrombolysis in the presence of microbubbles on clot composition. Using an established *ex vivo* model of thrombosis, we assessed the thrombolytic efficacy of rt-PA, 120 kHz continuous-wave (CW) ultrasound, and circulating microbubbles (Definity®; Lantheus Medical Imaging; Billerica, MA USA) on two distinct types of whole-blood clots. Further, we employed routine histological evaluation and scanning electron microscopy (SEM) to characterize differences in composition between the two clot types. These results, in the context of mechanistic and clinical investigations of UET, will be discussed.

Materials and Methods

Whole-Blood Clot Formation

Porcine venous blood was collected aseptically from donor hogs (Lampire Biologicals; Pipersville, PA USA), anticoagulated with a citrate-phosphate-dextrose solution (final concentration in blood: 16.1 mM Na-citrate, 17.6 mM d-glucose, 1.96 mM citric acid, and 2.3 mM NaH_2PO_4) and shipped on ice overnight to the University of Cincinnati. Porcine blood is a good alternative to human blood for thrombolysis research due to its availability, price, and biochemical similarity to human blood (Pond and Mersmann 2001). Before coagulation, the blood was placed on a laboratory stirrer for 15 minutes and incubated at 37.3 °C for 20 minutes while exposed to room air to equilibrate gas content. To induce coagulation, the blood was recalcified with $CaCl_2$ to a final concentration of 16.1 mM and pipetted into glass Pasteur pipets Fisher Scientific; Pittsburgh, PA USA). The pipets were incubated at 37.3 °C for three hours during coagulation, and placed in a laboratory refrigerator at 4 °C for a minimum of three days before experimental treatment to allow for consistent clot retraction. These methods of clot formulation are similar to those implemented in other thrombolysis studies, and result in clots with appreciable lytic rates and consistent lytic susceptibility, which is imperative in mechanistic sonothrombolysis studies (Emelianov et al. 2002; Shaw et al. 2009; Holland et al. 2002; Datta et al. 2006; Meunier et al. 2007; Roessler et al. 2011).

The clot formation protocol was performed using two different types of Pasteur pipets, borosilicate and flint glass, to stimulate the coagulation cascade to different degrees. This resulted in different types of whole-blood clots (Figure 1), which were subjected to a combination treatment of intermittent, 120 kHz CW ultrasound with rt-PA and microbubbles. Borosilicate glass, a highly hydrophilic surface, produced stiff, retracted whole-blood clots, while flint glass produced softer, unretracted whole-blood clots. These qualitative observations are consistent with previous investigations of clot retraction by Faxalv et al. (2008). After the three-day retraction period, the interior of the Pasteur pipets contained the whole-blood clot (solid phase), transluscent serum (fluid phase), and uncoagulated whole blood. The volume of the fluid phase was likely a result of syneresis, an effect first studied in blood clots by Pickering and Hewitt (1923).

Histology and Image Analysis

Eighteen cylindrically shaped clots (nine retracted and nine unretracted) were produced *in vitro* as indicated above for microscopic image analysis. Each clot was removed from its respective Pasteur pipet, trimmed to 1 cm in length, and fixed in 10% neutral buffered formalin for 24 hours. Clots were submitted for paraffin processing through a series of graded alcohol and xylene steps; all samples were subsequently bisected and paraffin embedded. Five μm-thick tissue sections were obtained from each paraffin block and stained with hematoxylin and eosin (H&E). Stained sections were subjected to qualitative and quantitative histologic evaluation under bright-field microscopy. Histologic sections were photographed at 20X magnification with an Olympus BX61 microscope equipped with a color digital camera (Olympus DP70, 12.5 megapixel resolution; Center Valley, PA USA). Image analysis data were processed with a custom-written MATLAB (The Mathworks Inc.; Natick, MA USA) image analysis routine that determined the total amount of open white space present in each image. Using binary pixel intensity thresholding, the total number of white pixels present in an image was summed, and this value was divided by the total number of pixels in the image to determine percent white space. The total number of white pixels was used to describe the extent of clot retraction and porosity.

Scanning Electron Microscopy

To characterize compositional properties, clots were processed in a similar manner to the method described by Weisel et al. (Weisel and Nagaswami 1992) and subjected to routine SEM. All materials used for clot processing were obtained from Electron Microscopy Sciences (Hatfield, PA USA) and dilutions made with 0.2 μm-filtered deionized water. Following the three-day retraction period, clots were rinsed with cold phosphate-buffered saline (PBS, Sigma Aldrich Co.; St. Louis, MO USA) and axially sectioned for processing. The sections were fixed with 2% (v/v) glutaraldehyde in cacodylate buffer overnight. Following fixation, the samples were rinsed twice with 0.1 M cacodylate buffer and post-stained with 1% (v/v) osmium tetroxide to enhance surface imaging contrast. Following two saline rinses, the clots were dehydrated with a series of 15 minute graded ethanol steps (v/v; 50%, 50%, 70%, 70%, 95%, 100%) and left in 100% ethanol overnight. Finally, the clots were chemically dried with pure propylene oxide and allowed to air dry in a fume hood. Immediately prior to imaging, the samples were sputter-coated with gold-palladium under argon for 90 seconds to confer surface conductivity. SEM imaging was performed on axial sections from eight clot samples (four retracted and four unretracted clots from different porcine subjects). High-resolution (650-6500X magnification) images were captured of random positions on the axial section surfaces of each clot. In addition to differences in surface composition between the two clot models, qualitative differences were observed between the interior and the superficial surface (outside edge) of each clot. Thus, images of these surfaces were collected and analyzed separately.

Two blinded observers assessed the fibrin content and fiber diameter of each sample using routines written in MATLAB and ImageJ (National Institutes of Health; Bethesda, MD USA). To determine fibrin content, each observer selected a region of interest (ROI) on each image (3500X) devoid of red blood cells. Thereafter, linear contrast adjustment and binary thresholding were performed until the fibrin on the surface of each image was highlighted. *Percent fibrin* was calculated by dividing the number of highlighted fibrin pixels by the total number of pixels in the ROI. To determine *fiber diameter*, each observer was presented with a new, randomly chosen 150 × 150 pixel ROI. The diameter of the fiber closest to five randomly chosen locations within the ROI was measured and recorded by the observer (n = 83).

Ex Vivo Carotid Perfusion System

Thrombolysis experiments in the *ex vivo* arterial thrombosis system were conducted as previously described (Hitchcock et al. 2011). Briefly, carotid arteries were excised from mature hogs at an abattoir within one hour of exsanguination in accordance with University of Cincinnati Institutional Animal Care and Use Committee guidelines for post-mortem studies and transported to the University of Cincinnati for mounting in the *ex vivo* system. The perfusion system, depicted in Figure 2, consisted of a closed loop that circulated sodium-citrate anticoagulated porcine plasma (Lampire Biologicals; Pipersville, PA USA) with a pulsatile blood pump (Harvard Apparatus; Holliston, MA USA). Porcine plasma was chosen as the perfusate because it contains the proteins vital to intrinsic fibrinolysis while avoiding the confounding effects that erythrocytes introduce on ultrasound scattering and mass deposition within the clot sample.

Experimental Treatment

For each experiment, the sample holder was mounted within the system as follows. First, a carotid artery was trimmed to 4.5 cm and placed under physiologic pressure (90 – 100 mmHg) with PBS and inspected for side branches and gross leaks. If necessary, side branches were sutured with 4.0 braided silk suture (Deknatel; Research Triangle Park, NC USA). The distal end of the intact carotid artery was mounted to a 3 mm inner-diameter

barbed, polypropylene cannula (Cole Parmer Instrument Company; Vernon Hills, IL USA) and secured with 3.0 nylon surgical suture (Look Surgical Specialties; Reading, PA USA). Next, a clot was gently washed with PBS, trimmed to 3.5 cm in length, blotted, weighed, and injected proximally into the carotid artery. The proximal end of the artery was secured to the upstream cannula with a nylon suture. Additionally, a small 30 Gauge hole was made in the downstream cannula prior to artery mounting to act as a flow bypass in the event that the clot completely clogged the downstream cannula during treatment. This scenario also occurs *in vivo*, as collateral branches of the thrombosed cerebral arteries often maintain residual flow of fibrinolytics into the ischemic region (Alexandrov et al. 2010). To provide the artery with a physiological perivascular fluid, the artery was bathed in degassed (<35%), artificial cerebrospinal fluid (aCSF) contained separately from the tank water by an unlubricated latex condom.

The thrombolytic drug, rt-PA (Genentech; South San Francisco, CA USA), was reconstituted with 0.2 μm-filtered, deionized water to a concentration of 1 mg/ml, aliquoted into polyproylene cryovials, and frozen until use at −80 °C. Definity® vials were activated according to manufacturer instructions and used within 3 days. To preserve the composition of headspace gas, the Definity® vials were vented to octofluoropropane (C_3F_8) at 20 °C and one atmosphere of pressure as described by Prokop et al (2007).

At the beginning of each trial, a 10 mL syringe containing porcine plasma, porcine plasma with 7.88 μg/mL rt-PA, or porcine plasma with 7.88 μg/mL rt-PA and 0.70 μl/mL Definity® was infused proximally at a flow rate of 0.6 ml/min. A flow clamp, located distal to the sample holder, was adjusted manually throughout the trial to maintain a luminal flow rate of 1.5 ml/min. These infusion and luminal flow rates were selected to obtain a rt-PA concentration of 3.15 μg/mL (Meunier et al. 2007a; Tanswell et al. 1991). Definity® was infused to obtain a luminal concentration of 0.28 μL/mL, which is the highest concentration predicted theoretically assuming the manufacturer recommended “venous bolus injection” and a perfluorocarbon clearance rate of 5 μL/min. To obtain this concentration, a monoexponential function describing the half-life of Definity® in the body (Lantheus Medical Imaging; Definity® microbubble insert) was convolved with a function simulating a typical bolus injection regime. The microbubbles were assumed to disperse homogenously within a five liter blood volume, during an 11 second bolus injection, which is consistent with clinical protocol for Definity® infusions performed at University Hospital in Cincinnati, OH for left-ventricular opacification.

Thrombolytic efficacy, determined by percent mass loss over the 30-minute treatment periods, was individually determined for retracted and unretracted clots. Although alternative metrics of thrombolytic efficacy have been proposed, such as d-dimer concentration (Alonso et al. 2009), fractional clot width (Meunier et al. 2007b), and photoabsorbance (Westlund and Andersson 1985), mass loss measurement is a simple experimental technique that is minimally susceptible to inter-sample variability, and is a chief concern for physicians treating acute ischemic stroke (Shaw et al. 2009). Additionally, alternative methods would have been difficult to implement in this *ex vivo* model-- porcine d-dimer assay kits are not commercially available, and light absorbance by the *ex vivo* carotid artery would have confounded clot width and photoabsorbance measurements prohibitively.

Model Parameters

The physiologic parameters monitored during the course of experimental treatment (fluid pressure, temperature, oxygen concentration, flow rate, pH) did not vary significantly between trials ($p > 0.05$). Table 1 outlines these data, which are presented as the data mean ±

SD. The inline flow rate was measured experimentally to be 1.42 ± 0.08 mL/min, which indicates an effective average luminal rt-PA concentration of 3.33 ± 0.18 μg/mL.

Ultrasound Therapy

The ultrasound therapy was designed to mimic extravascular insonation of an intracranial thrombus located in the middle cerebral artery. The test segment was submerged in a tank filled with degassed, deionized water containing two circular single-element ultrasound transducers used for ultrasound therapy and passive cavitation detection. This experimental setup is depicted in Figure 3. Prior to each experiment, a calibrated 120-kHz therapy transducer (Sonic Concepts; Bothell, WA USA) was aligned orthogonally and confocally with a 2.25 MHz passive cavitation detector (Picker Roentgen GmbH; Espelkamp, Germany) using an ultrasonic pulser receiver (Panametrics 5077PR, Olympus NDT Inc.; Waltham, MA USA). The confocal point was positioned 8 mm downstream from the face of the clot for each experiment using a three axis-translation stage (Newport 423; Irvine, CA USA). This geometry was chosen to ensure that the ultrasound pressure amplitude across the clot profile was sufficient to induce stable cavitation, based on previous threshold measurements performed in this system (Hitchcock et al. 2011) and on the *in situ* pressure profile of the ultrasound therapy transducer seen in Figure 4. During experimental treatment, an RF function generator (Agilent Technologies Inc.; Santa Clara, CA USA) supplied a continuous-wave sinusoidal signal that was amplified (Amplifier Research, 750A250; Souderton, PA USA) and impedance-matched (custom matching network, Sonic Concepts Inc.) to drive the 120-kHz therapy transducer. Acoustic scattering from the sample holder and polycarbonate cannulae distorted the beam profile slightly, so an *in situ* pressure calibration was performed in the absence of an artery and clot. A broadband hydrophone (0.5 mm, Reson Inc; Goletta, CA USA) was positioned in the anticipated axial center of the artery and advanced incrementally downstream to the outlet cannula, passing through the natural focus of the therapy transducer in its transverse plane (Figure 4, inset). Based on this calibration, the peak-to-peak acoustic pressure at the axial clot center was 0.48 MPa, which diminished to roughly 0.34 MPa at the upstream and downstream faces of the clot.

Retracted and unretracted clots were subjected individually to 120-kHz, continuous-wave ultrasound with intermittent pulsing. This scheme was designed to maximize the amount of stable cavitation occurring within the artery lumen during ultrasound treatment. Details describing the rationale and development of this technique were previously described by Hitchcock et al (2011).

Passive Cavitation Detection

Acoustic emissions detected within the sensitive region of a calibrated 2.25 MHz passive cavitation detector were amplified with a wideband voltage preamplifier (Signal Recovery Model 5185; Oak Ridge, TN USA) and saved on a digital oscilloscope (Lecroy Corporation; Santa Clara, NY USA). Twenty millisecond voltage traces were stored every second and postprocessed in MATLAB to analyze spectral content, consistent with the methods of Datta et al. (2006). Ultraharmonic power, represented in the signal at odd integers of half the insonating frequency, indicated the presence of stable cavitation, which is associated with fluid microstreaming (Doinikov and Bouakaz 2010; Collis et al. 2010a). Broadband signal power indicated the presence of inertial cavitation, or bubble collapse from large radial excursions, which is associated with microjetting (Chen et al. 2012). Stable and inertial cavitation correspond to acoustic emissions within these respective frequency ranges (Coussios and Roy 2008; Leighton 1997), and have been the focus of a number of studies investigating the mechanism of ultrasound-enhanced thrombolysis (Hitchcock et al. 2011) and drug delivery (Hynynen and Clement 2007; Choi et al. 2007; Hallow et al. 2007;

McDannold et al. 2005; Hitchcock et al. 2010; Radhakrishnan et al. 2005; Haworth et al. 2012; Husseini et al. 2005).

Data Analysis and Statistical Methods

Statistical analysis was performed using the MATLAB Statistical Toolbox. Differences in means between experimental treatments were determined by one-way unbalanced ANOVA with an alpha level of 0.05. Subsequent unpaired Student t-tests with an alpha level of 0.025 were used to discern statistically significant differences between individual treatments. The data mean, standard deviation, p-value, t-statistic, and degrees of freedom (mean ± SD; p, t-stat, DF) are reported for each statistical comparison.

Two observers, blinded to the clotting technique, were chosen to conduct the analysis of scanning electron microscopy images. Each observer had previous experience in medical image analysis and clot characterization. Lilliefore's test for normality was performed and p-values below 0.05 indicated significant deviations from normality. A Wilcoxon rank-sum test was performed to determine significant differences between medians at an alpha level of 0.05.

Results

Histology

Microscopic analysis of H&E-stained sections showed consistent qualitative differences in pattern between both clot types (Figure 5). Retracted clots produced in borosilicate pipettes appeared homogenous and displayed very densely packed RBCs allowing only scant amounts of fibrin to be visible. In some sections, fibrin was observed in thicker strands or accumulations. Conversely, unretracted clots produced in flint glass pipettes displayed loosely aggregated RBCs with a loose fibrin network often visible around the RBCs. In addition, this clot model showed considerable spacing (devoid of either fibrin or RBCs) relatively homogenously distributed between the RBCs. Image analysis performed on H&E images revealed that this intercellular spacing comprised 3.45 ± 2.17% of unretracted clots, and only 0.87 ± 0.95% of retracted clots, which was a significant difference ($p \ll 0.01$, t-stat = 4.69, DF = 34).

Scanning Electron Microscopy

Qualitative and quantitative analysis of SEM images also revealed considerable differences in compositional properties between the two clot models. Representative SEM images of the interior of each clot type are depicted in Figure 6. These images illustrate the disparity in fibrin content present within the clot interior. Superficial fibrin content was significantly greater ($p = 0.015$) in retracted (73.8%) compared to unretrated clots (54.6%). Box and whisker plots of these data on the superficial surface of the clots, depicting the median, first and third quartile ranges, and data extrema are also depicted in Figure 6. Differences in fiber diameter in retracted and unretracted clots, respectively, were not significant. Superficial fibers had a mean diameter of 0.173 μm in retracted clots and 0.169 μm in unretracted clots ($p = 0.18$). Interior fibers had a mean diameter of 0.232 μm in retracted clots and 0.253 μm in unretracted clots ($p = 0.97$). Echinocyte formations were also observed in the erythrocyte population within SEM images. This is a known artifact of clot storage and aging, and is a result of dehydration, increased pH, and decreased ATP concentration (Reinhart and Chien 1987).

Clot Fluid Phase Estimation

To aid in clot characterization, the volume of the fluid phase (expressed as a percentage of total volume ± one standard deviation) was measured in sixteen clots (eight retracted, eight

unretracted) immediately after removal from each respective Pasteur pipet. For unretracted clots, this value was 58.2 ± 6.7%, which was significantly greater than in retracted clots (10 ± 8.7%; $p \ll 0.05$; t-stat = 12.4, DF = 14).

Ex Vivo Thrombolysis

During treatment, clots lysed in both the axial and radial directions. After treatment and blotting, visual inspections indicated that lysis was most apparent in the longitudinal direction. Considerable radial lysis occurred at the upstream portion of the clots, resulting in conical-shaped residual clots during the most efficacious treatments.

The thrombolytic efficacy of each treatment is depicted in Figure 7. Reported values correspond to the mean ± one standard deviation (SD). Retracted clots subjected to control treatments (porcine plasma alone) lost a minimal amount of mass during the thirty-minute treatment period (8.8 ± 1.8%). Exposure to 3.15 μg/mL rt-PA increased mass loss significantly ($p \ll 0.01$; t-stat = 5.73, DF = 11) compared to control treatment (17.1 ± 2.6% vs. 8.8 ± 1.8%). However, when retracted clots were exposed to rt-PA, Definity®, and 120 kHz, no increase in mass loss (p = 0.28; t-stat = 1.14, DF = 10) occurred (17.1 ± 2.6% vs. 19.6 ± 4.7%). Unretracted clots lysed much more effectively during control treatments (44.9 ± 4.0%) than retracted clots. Exposure to rt-PA improved thrombolytic efficacy further (53.5 ± 4.5; p = 0. 009, t-stat = 3.29, DF = 10). Co-administration of rt-PA, Definity® and ultrasound resulted in further significant increases in thrombolytic efficacy (73.2 ± 4.7%; $p \ll 0.01$, t-stat = 11.14, DF = 11). These data indicate that rt-PA improves thrombolytic efficacy significantly in both clot models compared to control treatment. However, when rt-PA was augmented with Definity® and intermittent US exposures, thrombolytic efficacy only increased in the unretracted clots.

Cavitation Detection

Figure 8 depicts the detected energies from spectral analysis of acoustic emissions. In general, the amounts of stable and inertial cavitation, indicated by the spectral power at ultraharmonic and broadband frequencies, respectively, decayed in time during each 19.5-second intermittent CW pulse. Broadband activity was strong within the first acquired trace of each pulse. However, these emissions decayed rapidly, diminishing to baseline within the first few seconds. For rt-PA, Definity® + US treatments, the average amount of ultraharmonic and broadband energy detected by the PCD was greater in the retracted clots, however the differences were insignificant ($p \gg 0.05$; t-stat < 1.1; DF = 11). Since unretracted clots were, in general, larger in volume than retracted clots, the number of Definity microbubbles flowing through the sensitive region of the detector was greater in the case of retracted clots. Acoustic emissions from the PCD were also processed for four clots (two plasma alone and two rt-PA treatments) to establish a baseline level of ultraharmonic and broadband activity when ultrasound was not applied. These energies were $3.5 \times 10^{-7} \pm$ and $3.9 \times 10^{-7} \pm V^2 \times s$, respectively.

Discussion

Retracted thrombi have increased resistance to rt-PA thrombolysis. We investigated this dependence in the context of ultrasound-enhanced thrombolysis. Thrombolytic enhancement, defined by an increase in clot mass loss, was observed in the presence of microbubbles undergoing stable nonlinear oscillations, or stable cavitation. However, thrombolytic enhancement compared to sham treatment with rt-PA alone was observed only when unretracted whole-blood clots were exposed to rt-PA, 120 kHz ultrasound, and microbubbles. Within the two clot models, no significant differences were detected in the total amount of stable or inertial cavitation activity occurring within the artery lumina. Thus,

the lack of thrombolytic enhancement within retracted clots was most likely caused by some difference in their composition, which prohibited a higher thrombolytic rate with US and microbubbles. These results imply a correlation between the compositional properties of clot and sonothrombolysis. Further investigation of this relationship could assist physicians in their clinical decisions about the use of rt-PA and sonothrombolysis.

Compositional analysis by SEM and H&E revealed that retracted clots contained a denser fibrin network compared to retracted clots that exhibited thrombolytic enhancement. Superficial fiber diameters were approximately 30% smaller than those analyzed within the clot, regardless of clot model. The decreased fiber diameters on the exterior of the clots could have been due to differences in thrombin concentration (Weisel 2007) or erythrocyte density (Gersh et al. 2009) between the clot surface and interior during formation. However, no differences in superficial or interior fiber diameters between the clot models were evident and likely did not contribute to a difference in the sonothrombolytic susceptibility.

The dependence of sonothrombolysis on clot retraction has interesting mechanistic implications. Reduction in clot volume reduces pore size and expels blood plasma from pores within the fibrin network, resulting in a lower concentration of fibrinolytics such as t-PA and plasminogen within the clot (Sabovic et al. 1990). Kunitada et al. (1992), in their studies of platelet-rich clots, concluded that thrombolysis was inhibited by the degree of platelet-mediated clot retraction, which they attributed to a reduction in clot-bound plasminogen. In our study, a non-pharmacological technique was used to stimulate maximal platelet activation and clot retraction. Consistent with Kunitada et al., our results indicate that cavitation-enhanced thrombolysis could depend on clot-bound plasminogen. Using pulsed diagnostic ultrasound to accelerate clot lysis with Definity® microbubbles, Xie et al. (2011) observed a reduction in thrombolytic efficacy as the clot aged from three to six hours. Plasminogen decreases in concentration within the clot with aging and necessitates an external source for further lysis. Combined, these results suggest that changes in clot architecture and plasminogen content affect the efficacy of oscillating microbubbles in accelerating thrombolysis.

Our results suggest three possible scenarios that may be necessary for thrombolytic enhancement with ultrasound. First, the concentration of plasminogen within a clot during lysis may have to exceed some critical threshold. This scenario is compelling because the kinetic rate of t-PA fibrinolysis decreases steadily with plasminogen concentration (Westlund and Andersson 1985). A plasminogen threshold would also depend on plasma rt-PA concentration, because higher concentrations of the fibrinolytic enzyme would not produce a higher rate of lysis. Secondly, the plasminogen distribution near the surface of the clot must be sufficiently deep to facilitate lysis in non-superficial layers. The plasminogen content in retracted clots during lysis localizes to the superficial fibrin layers less than 50 μm from the clot surface, and at much lower concentrations than in unretracted clots (Sakharov et al. 1996). In this scenario, the presence of fibrin degradation products near the clot surface could limit rt-PA access to plasminogen within the clot. In our whole-blood clot model, the low thrombolytic rate observed in retracted clots most likely occurred due to a low rate of erythrocyte liberation, because a significant portion of a clot's mass can be attributed to dense formed elements (Liebeskind et al. 2011). Therefore, micromixing by cavitating microbubbles must have contributed minimally to further fibrin degradation product removal in the presence of plasma flow. In the case of unretracted clots, the high rate of erythrocyte liberation may have congested the superficial binding sites for rt-PA and plasminogen. Microstreaming, known to occur near surfaces during bubble oscillation (Collis et al. 2010b), could facilitate this removal and allow for accelerated fibrinolysis. Thirdly, the porosity of the clot must be sufficient to allow increased penetration of fibrinolytics by cavitation. Here, thrombolytic enhancement was observed when unretracted

clots, composed of loosely aggregated fibrin and spaces devoid of particulate, were exposed to ultrasound, microbubbles, and rt-PA. Future studies should focus on studying each of these effects specifically in appropriate *in vitro* models.

The data presented here are also consistent with clinical and *in vitro* thrombolysis trials. Molina et al. (2004), in their studies of thrombolytic efficacy and clinical outcomes as a function of clot subtypes, concluded that clots of acute cardioembolic origin lysed more easily and resulted in better clinical outcomes than clots from large vessel disease. Large vessel thrombosis is concomitant with significant clot retraction, due to accumulations of platelet aggregates (Weisel and Litvinov 2008; Francis et al. 1983) on the clot surface. Both clot types in this study would likely occur *in vivo* during ischemic stroke, as evidenced by the large variation in erythrocyte and fibrin composition in thrombi retrieved from middle cerebral artery occlusions (Liebeskind et al. 2011).

In this study, both clot models were erythrocyte-rich, but differed in the extent of fibrin networking within their interior. Clots formed in highly hydrophilic borosilicate glass experienced significant clot retraction during *in vitro* manufacturing. Retracted clots have been shown to lyse much less effectively, regardless of treatment, compared to unretracted clots (Blinc et al. 1991, Francis et al. 1992). These results can likely be attributed to the lack of dense fibrin matrix formation throughout unretracted clots (Figures 5 & 6), and the paucity of plasminogen present within retracted clots (Sabovic et al. 1990). In unretracted clots subjected to plasma alone treatments, the small amount of t-PA present endogenously in porcine plasma (~8ng/mL) (Jern et al. 1997) may have had a significant effect on lysis, compared to retracted clots. The lack of significant thrombolytic enhancement observed in sonothrombolysis trials with microbubbles (Molina et al. 2009) may also be explained by the data presented here. Some clots, depending on their etiology and vascular origin, may be predisposed to sonothrombolytic susceptibility depending on the concentration of plasminogen bound within the fibrin matrix. Consistent with this hypothesis, *in vitro* studies have proposed delivering plasminogen to the site of occlusion concomitantly with rt-PA (Meunier et al. 2011).

Previous sonothrombolysis investigations are also consistent with the results presented here. Using clots manufactured in silicone-coated glass tubes, Datta (2007) observed significant thrombolytic efficacy enhancement in the presence of stable cavitation and rt-PA. Silicone is often used as a coating in blood collection tubes to prevent cell adherence by rendering the glass surface hydrophobic. Clots formed in these types of tubes experience incomplete clot retraction, and are most likely more susceptible to sonothrombolysis. In their *ex vivo* thrombolysis studies using clots manufactured asceptically after exsanguination at a local abattoir, Hitchcock et al. (2011) observed significant thrombolysis enhancement in the presence of rt-PA and cavitating microbubbles. Based on past experience in this laboratory, clots formed in this manner are much softer and friable, and most likely do not experience robust clot retraction.

Though compelling mechanistic conclusions can be drawn from studies in this *ex vivo* thrombosis model, its limitations should be mentioned. As discussed by Hitchcock et al. (2011), the cell signaling that occurs within the cardiovascular system of an organism during acute ischemic stroke is mostly absent in this *ex vivo* model. While intact vascular endothelial cells of excised carotid arteries remain capable of responding to strong vascular agonists (Weintraub et al. 1994), their ability to produce antithrombotic cofactors in response to ischemia or thrombosis diminishes after removal from the live animal and hypothermal storage (Parolari et al. 2002). To mitigate this effect, we chose to perfuse the *ex vivo* artery with porcine plasma saturated with oxygen (> 30 mg/L), which is greater than that in ischemic tissue (Ogawa et al. 1990). Yet, these studies have also shown that

endothelial cells, cultured in ischemic conditions, exhibit prothromotic tendencies and increase permeability to the vascular tunics. Though this *ex vivo* model has limitations, it does provide a quasi-realistic environment to simulate thrombosis while testing the thrombolytic efficacy of well-characterized sonothrombolysis treatments.

Conclusions

In conclusion, the data presented here demonstrate that sonothrombolysis is difficult to achieve with retracted clots. The mechanism of this inhibition is unclear, but may be related to clot structure and/or biochemical composition. Future *in vitro* and *in vivo* studies should focus on clot characteristics when designing thrombolytic treatment strategies using rt-PA, microbubbles, and ultrasound.

Acknowledgments

The authors would like to acknowledge Marepalli Rao, Ph.D. for his support with statistical analysis, Jason L. Raymond, M.S. for his assistance with flow system components, and Stehlin Meats (Colerain, OH USA) for providing porcine carotid tissue. Financial support was provided by NIH R01 NS047603.

References

Alexandrov A. Current and future recanalization strategies for acute ischemic stroke. Journal of Internal Med. 2010; 267:209–19. [PubMed: 20175867]

Alexandrov A, Tsivgoulis G, Rubiera M, Vadikolias K, Stamboulis E, Molina C, Alexandrov A. End-Diastolic Velocity Increase Predicts Recanalization and Neurological Improvement in Patients With Ischemic Stroke With Proximal Arterial Occlusions Receiving Reperfusion Therapies. Stroke. 2010; 41:948–52. [PubMed: 20224054]

Alexandrov AV, Molina CA, Grotta J, Garami Z, Ford SR, Alvarez-Sabin J, Montaner J, Saqqur M, Demchuk AM, Moya L, Hill MD, Wojner AW, Investigators C. Ultrasound-enhanced systemic thrombolysis for acute ischemic stroke. New Engl J Med. 2004; 351:2170–8. [PubMed: 15548777]

Alonso A, Dempfle C, Della Martina A, Stroick M, Fatar M, Zohsel K, Allamann E, Hennerici M, Meairs S. In vivo clot lysis of human thrombus with intravenous abciximab immunobubbles and ultrasound. Thromb Res. 2009; 124:70–4. [PubMed: 19349068]

Blinc A, Kennedy SD, Bryant RG, Marder VJ, Francis CW. Flow through clots determines the rate and pattern of fibrinolysis. Thromb Haemostasis. 1994; 71:230–5. [PubMed: 8191404]

Blinc A, Planinsic G, Keber D, Jarh O, Lahajnar G, Zidansak A, Demsar F. Dependence of blood clot lysis on the mode of transport of urokinase into the clot--a magnetic resonance imaging study in vitro. Thromb Haemostasis. 1991; 65:549–52. [PubMed: 1871717]

Chen H, Brayman A, Evan A, Matula T. Preliminary observations on the spatial correlation between short-burst microbubble oscillations and vascular bioeffects. Ultrasound Med Biol. 2012 In Press.

Choi JJ, Pernot M, Small SA, Konofagou EE. Noninvasive, transcranial and localized opening of the blood-brain barrier using focused ultrasound in mice. Ultrasound Med Biol. 2007; 33:95–104. [PubMed: 17189051]

Collis J, Manasseh R, Liovic P, Tho P, Ooi A, Petkovic-Duran K, Zhu Y. Cavitation microstreaming and stress fields created by microbubbles. Ultrasonics. 2010a; 50:279.

Coussios CC, Roy RA. Applications of Acoustics and Cavitation to Noninvasive Therapy and Drug Delivery. Annu Rev Fluid Mech. 2008; 40:395–420.

Datta, S. Doctoral Dissertation. University of Cincinnati; Cincinnati, Ohio: 2007. The role of cavitation in enhancement of rt-PA thrombolysis.

Datta S, Coussios CC, McAdory LE, Tan J, Porter T, De Courten-Myers G, Holland CK. Correlation of cavitation with ultrasound enhancement of thrombolysis. Ultrasound Med Biol. 2006; 32:1257–67. [PubMed: 16875959]

Datta S, Coussios C, Ammi AY, Mast TD, de Courten-Myers G, Holland CK. Ultrasound-enhanced thombolysis using Definity as a cavitation nucleation agent. Ultrasound Med Biol. 2008; 34:1433.

Doinikov AA, Bouakaz A. Acoustic microstreaming around an encapsulated particle. J Acoust Soc Am. 2010; 127:1218. [PubMed: 20329820]

Emelianov SY, Chen X, O'Donnell M, Knipp B, Myers D, Wakefield TW, Rubin JM. Triplex ultrasound: elasticity imaging to age deep venous thrombosis. Ultrasound Med Biol. 2002; 28:757–67. [PubMed: 12113788]

Faxalv L, Tengvall P, Lindahl T. Imaging of blood plasma coagulation and its propagation at surfaces. J Biomed Mater Res. 2008; 85:1129–34.

Fox J, Phillips D. Polymerization and organization of actin filaments within platelets. Semin Hematol. 1983; 20:243–60. [PubMed: 6316555]

Francis CW, Blinc A, Lee S, Cox C. Ultrasound accelerates transport of recombinant tissue plasminogen activator into clots. Ultrasound Med Biol. 1995; 21:419–24. [PubMed: 7645133]

Francis CW, Markham RE Jr, Barlow GH, Florack TM, Dobrzynski DM, Marder VJ. Thrombin activity of fibrin thrombi and soluble plasmic derivatives. J Lab Clin Med. 1983; 102:213–9. [PubMed: 6864071]

Francis CW, Onundarson PT, Carstensen EL, Blinc A, Meltzer RS, Schwarz K, Marder VJ. Enhancement of fibrinolysis in vitro by ultrasound. J Clin Invest. 1992; 90:2063–8. [PubMed: 1430229]

Gabriel DA, Muga K, Boothroyd EM. The effect of fibrin structure on fibrinolysis. J Biol Chem. 1992; 267:24259–63. [PubMed: 1447176]

Gersh K, Nagaswami C, Weisel JW. Fibrin network structure and clot mechanical properties are altered by incorporation of erythrocytes. Thromb Haemostasis. 2009; 102:1169–75. [PubMed: 19967148]

Gersh K, Edmondson K, Weisel J. Flow rate and fibrin fiber alignment. Thromb Haemostasis. 2010; 8:2826–8.

Hacke W, Kaste M, Bluhmki E, Brozman M, Dávalos A, Guidetti D, Larrue V, Lees KR, Medeghri Z, Machnig T, Schneider D, von Kummer R, Wahlgren N, Toni D. Thrombolysis with alteplase 3 to 4. 5 hours after acute ischemic stroke. New Engl J Med. 2008; 359:1317–29. [PubMed: 18815396]

Hallow DM, Mahajan AD, Prausnitz MR. Ultrasonically targeted delivery into endothelial and smooth muscle cells in ex vivo arteries. J Control Release. 2007; 118:285–93. [PubMed: 17291619]

Haworth JK, Mast DT, Radhakrishnan K, Burgess TM, Kopechek AJ, Huang S, McPherson DD, Holland KC. Passive cavitation imaging with pulsed ultrasound insonations. J Acoust Soc Am. 2012

Hitchcock KE, Caudell DN, Sutton JT, Klegerman ME, Vela D, Pyne-Geithman GJ, Abruzzo T, Cyr PEP, Geng Y, McPherson DD, Holland CK. Ultrasound-enhanced delivery of targeted echogenic liposomes in a novel ex vivo mouse aorta model. J Control Release. 2010

Hitchcock K, Ivancevich N, Haworth K, Caudell Stamper D, Vela D, Sutton J, Pyne-Geithman G, Holland C. Ultrasound-Enhanced rt-PA Thrombolysis in an ex vivo Porcine Carotid Artery Model. Ultrasound Med Biol. 2011; 37:1240–51. [PubMed: 21723448]

Holland CK, Vaidya SS, Coussios C, Shaw GJ. Thrombolytic effects of 120-kHz and 1-MHz ultrasound and tissue plasminogen activator on porcine whole blood clots. J Acoust Soc Am. 2002; 112:2370.

Holland CK, Vaidya SS, Datta S, Coussios C, Shaw GJ. Ultrasound-enhanced tissue plasminogen activator thrombolysis in an in vitro porcine clot model. Thromb Res. 2008; 121:663–73. [PubMed: 17854867]

Husseini GA, Diaz De La Rosa MA, Richardson ES, Christensen DA, Pitt WG. The role of cavitation in acoustically activated drug delivery. J Control Release. 2005; 107:253–61. [PubMed: 16046023]

Hynynen K, Clement GT. Clinical applications of focused ultrasound - The Brain. Int J Hyperther. 2007; 23:202.

Jern C, Seeman-Lodding H, Biber B, Winso O, Jern S. An experimental multiple-organ model for the study of regional net release/uptake rates of tissue-type plasminogen activator in the intact pig. Thromb Haemostasis. 1997; 78:1150–6. [PubMed: 9308769]

Kramer M, Van DW, Koch K, Ploegmakers J, Van DS, Henriques J, Baan J, Rittersma S, Vis M, Piek J, Tijssen J, De Winter R. Presence of Older Thrombus Is an Independent Predictor of Long-Term

Mortality in Patients With ST-Elevation Myocardial Infarction Treated With Thrombus Aspiration During Primary Percutaneous Coronary Intervention. Circulation. 2008; 118:1810–6. [PubMed: 18852369]

Kunitada S, FitzGerald GA, Fitzgerald DJ. Inhibition of clot lysis and decreased binding of tissue-type plasminogen activator as a consequence of clot retraction. Blood. 1992; 79:1420–7. [PubMed: 1547340]

Goldstein, Larry B. An overview based on AHA/ASA Guidelines Anonymous. Oxford, England: Wiley-Blackwell; 2009. A Primer on Stroke Prevention and Treatment.

Leighton, TG. The Acoustic Bubble. Waltham, MA: Academic Press; 1997.

Liebeskind D, Sanossian N, Yong W, Starkman S, Tsang M, Moya A, Zheng D, Abolian A, Kim D, Ali L, Shah S, Towfighi A, Ovbiagele B, Kidwell C, Tateshima S, Jahan R, Duckwiler G, Vinuela F, Salamon N, Villablanca J, Vinters H, Marder V, Saver J. CT and MRI Early Vessel Signs Reflect Clot Composition in Acute Stroke. Stroke. 2011; 42:1237–43. [PubMed: 21393591]

McDannold N, Vykhodtseva N, Raymond S, Jolesz FA, Hynynen K. MRI-guided targeted blood-brain barrier disruption with focused ultrasound: Histological findings in rabbits. Ultrasound Med Biol. 2005; 31:1527–37. [PubMed: 16286030]

Meunier JM, Holland CK, Lindsell CJ, Shaw GJ. Duty Cycle Dependence of Ultrasound Enhanced Thrombolysis in a Human Clot Model. Ultrasound Med Biol. 2007a; 33:576–83. [PubMed: 17337113]

Meunier JM, Holland C, Porter TM, Lindsell CJ, Shaw GJ. Combination treatment with rt-PA is more effective than rt-PA alone in an in vitro human clot model. Curr Neurovasc Res. 2011; 8:305–12. [PubMed: 22023612]

Molina CA. Imaging the clot: does clot appearance predict the efficacy of thrombolysis? Stroke. 2005; 36:2333–4. [PubMed: 16224076]

Molina CA, Barreto A, Tsivgoulis G, Sierzenski P, Malkoff M, Rubiera M, Gonzales N, Mikulik R, Pate G, Ostrem J, Singleton W, Manvelian G, Unger E, Grotta J, Schellinger P, Alexandrov AV. Transcranial ultrasound in clinical sonothrombolysis (TUCSON) trial. Ann Neurol. 2009; 66:28–38. [PubMed: 19670432]

Molina CA, Montaner J, Arenillas JF, Ribo M, Rubiera M, Alvarez-Saban J. Differential pattern of tissue plasminogen activator-induced proximal middle cerebral artery recanalization among stroke subtypes. Stroke. 2004; 35:486–90. [PubMed: 14707233]

Ogawa S, Gerlach H, Esposito C, Pasagian-Macaulay A, Brett J, Stern D. Hypoxia modulates the barrier and coagulant function of cultured bovine endothelium. Increased monolayer permeability and induction of procoagulant properties. J Clin Invest. 1990; 85:1090–8. [PubMed: 2156893]

Parolari A, Rubini P, Cannata A, Bonati L, Alamanni F, Tremoli E, Biglioli P. Endothelial damage during myocardial preservation and storage. ATS. 2002; 73:682–90.

Pickering JW, Hewitt JA. The syneresis of blood clots. Exp Physiol. 1923; 13:199–207.

Pond, WG.; Mersmann, HJ. Biology of the Domestic Pig. Cornell University Press; Ithaca, NY: 2001.

Prokop AF, Soltani A, Roy RA. Cavitational Mechanisms in Ultrasound-Accelerated Fibrinolysis. Ultrasound Med Biol. 2007; 33:924–33. [PubMed: 17434661]

Radhakrishnan K, Haworth JK, Huang S, Klegerman EM, McPherson DD, Holland KC. Stability of echogenic liposomes as a blood pool ultrasound contrast agent in a physiologic flow phantom. Ultrasound Med Biol. 2005

Reinhart WH, Chien S. Echinocyte-stomatocyte transformation and shape control of human red blood cells: Morphological aspects. Am J Hematol. 1987; 24:1–14. [PubMed: 2432778]

Roessler F, Ohlrich M, Marxsen J, Stellmacher F, Sprenger A, Dempfle C, Seidel G. The platelet-rich plasma clot: a standardized in-vitro clot formation protocol for investigations of sonothrombolysis under physiological flows. Blood Coagul Fibrin. 2011:1.

Sabovic M, Lijnen HR, Keber D, Collen D. Correlation between progressive adsorption of plasminogen to blood clots and their sensitivity to lysis. Thromb Haemostasis. 1990; 64:450–4. [PubMed: 2096491]

Sakharov DV, Nagelkerke JF, Rijken DC. Rearrangements of the fibrin network and spatial distribution of fibrinolytic components during plasma clot lysis. Study with confocal microscopy. J Biol Chem. 1996; 271:2133–8. [PubMed: 8567670]

Shaw GJ, Meunier JM, Huang SL, Lindsell CJ, McPherson DD, Holland CK. Ultrasound-enhanced thrombolysis with tPA-loaded echogenic liposomes. Thromb Res. 2009

Silvain J, Collet JP, Nagaswami C, Beygui F, Edmondson K, Bellemain-Appaix A, Cayla G, Pena A, Brugier D, Barthelemy O. Composition of Coronary Thrombus in Acute Myocardial Infarction. JACC. 2011; 57:1359–67. [PubMed: 21414532]

Tanswell P, Seifried E, Stang E, Krause J. Pharmacokinetics and hepatic catabolism of tissue-type plasminogen activator. Arzneimittel-Forschung. 1991; 41:1310–9. [PubMed: 1815534]

Weintraub NL, Joshi SN, Branch CA, Stephenson AH, Sprague RS, Lonigro AJ. Relaxation of porcine coronary artery to bradykinin. Role of arachidonic acid. Hypertension. 1994; 23:976–81. [PubMed: 8206638]

Weisel J, Nagaswami C. Computer modeling of fibrin polymerization kinetics correlated with electron microscope and turbidity observations: clot structure and assembly are kinetically controlled. Biophys J. 1992; 63:111–28. [PubMed: 1420861]

Weisel JW. Structure of fibrin: impact on clot stability. Thromb Haemostasis. 2007; 5 (Suppl 1):116–24.

Weisel JW, Litvinov RI. The biochemical and physical process of fibrinolysis and effects of clot structure and stability on the lysis rate. Cardiovasc Hematol Agents Med Chem. 2008; 6:161–80. [PubMed: 18673231]

Westlund LE, Andersson LO. Studies on the influence of reactants and buffer environment on clot lysis induced by human plasminogen activators. Thromb Res. 1985; 37:213–23. [PubMed: 4039077]

Xie F, Everbach EC, Gao S, Drvol LK, Shi WT, Vignon F, Powers JE, Lof J, Porter TR. Effects of Attenuation and Thrombus Age on the Success of Ultrasound and Microbubble-Mediated Thrombus Dissolution. Ultrasound Med Biol. 2011; 37:280–8. [PubMed: 21208727]

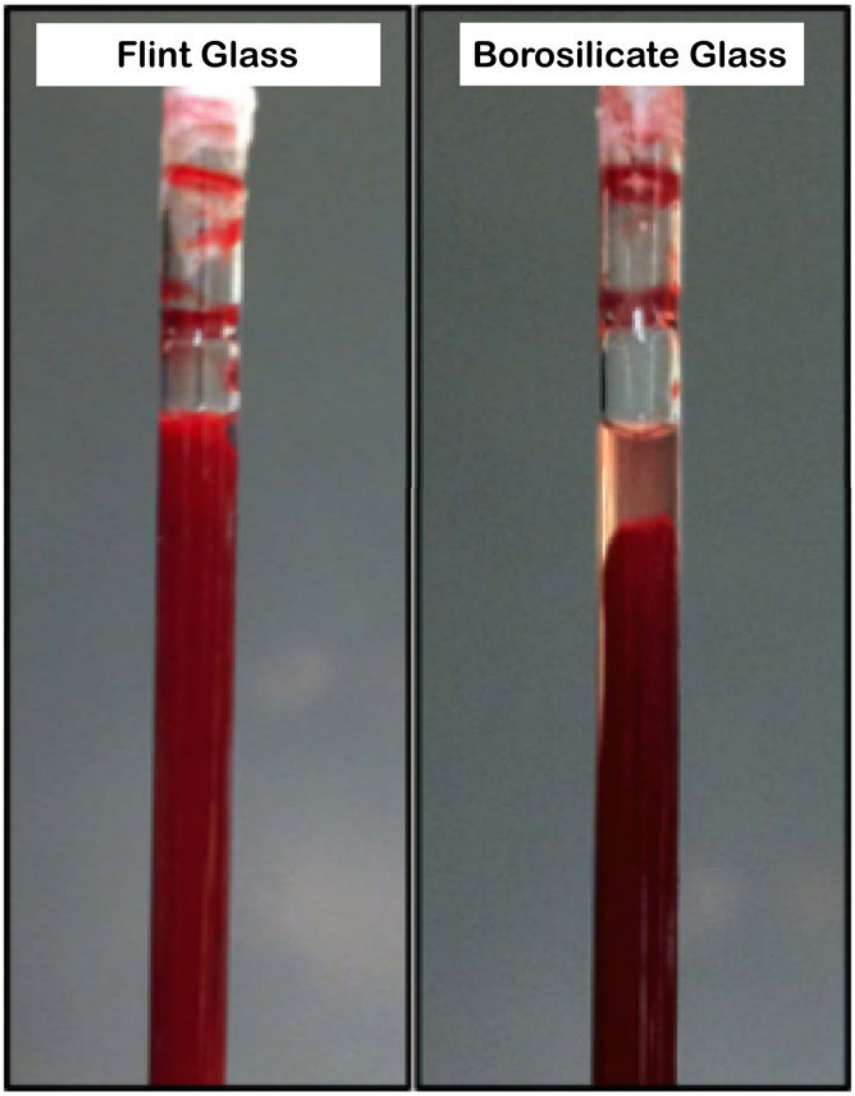

Figure 1.
Macroscopic views of each blood clot model prior to treatment. Left: unretracted clot in flint glass pipet, Right: retracted clot in borosilicate glass pipet.

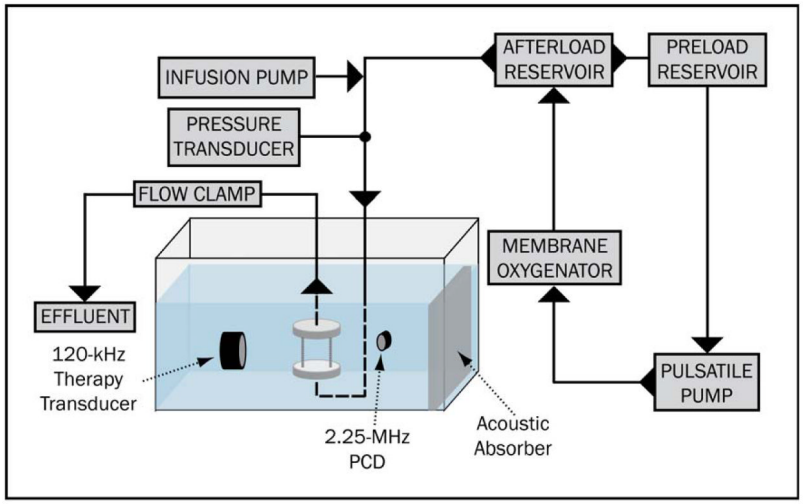

Figure 2.

The *ex vivo* thrombosis system. A custom-built sample holder (inset) allows perfusion of a clot-laden, living porcine carotid artery with oxygenated porcine plasma.

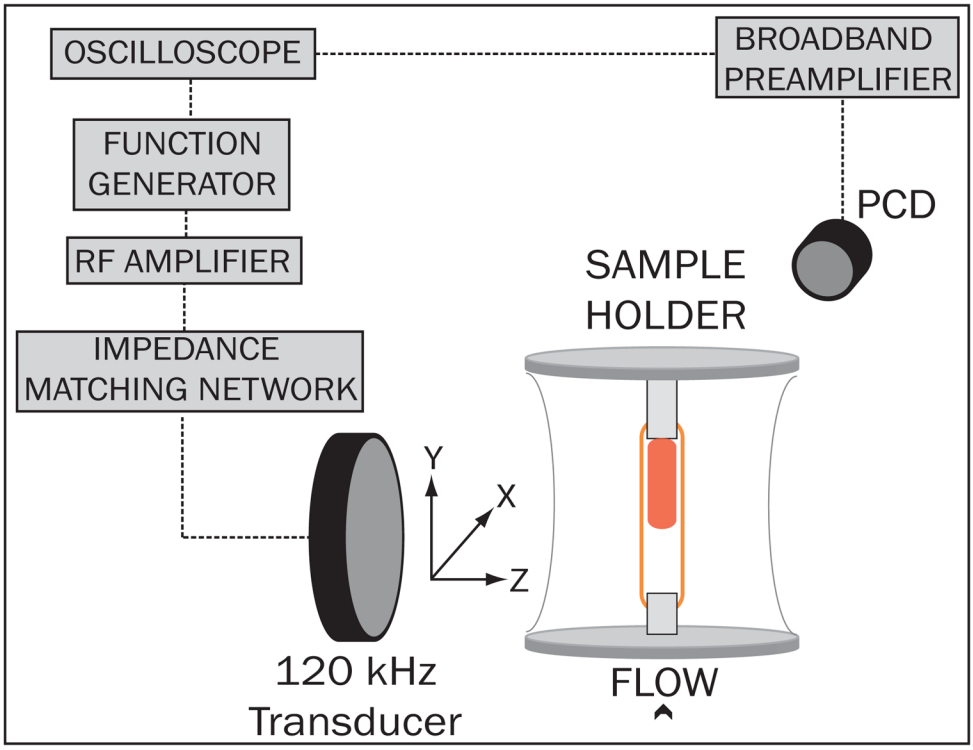

Figure 3.
Ultrasound alignment and send/receive electronic configuration. The focus of the 120 kHz therapy transducer was aligned 1.5 cm downstream of the thrombus center, to maximize the amount of stable cavitation occurring over the thrombus. The electronic signal from a passive cavitation detector, aligned at the upstream face of the thrombus, was amplified and recorded on an oscilloscope.

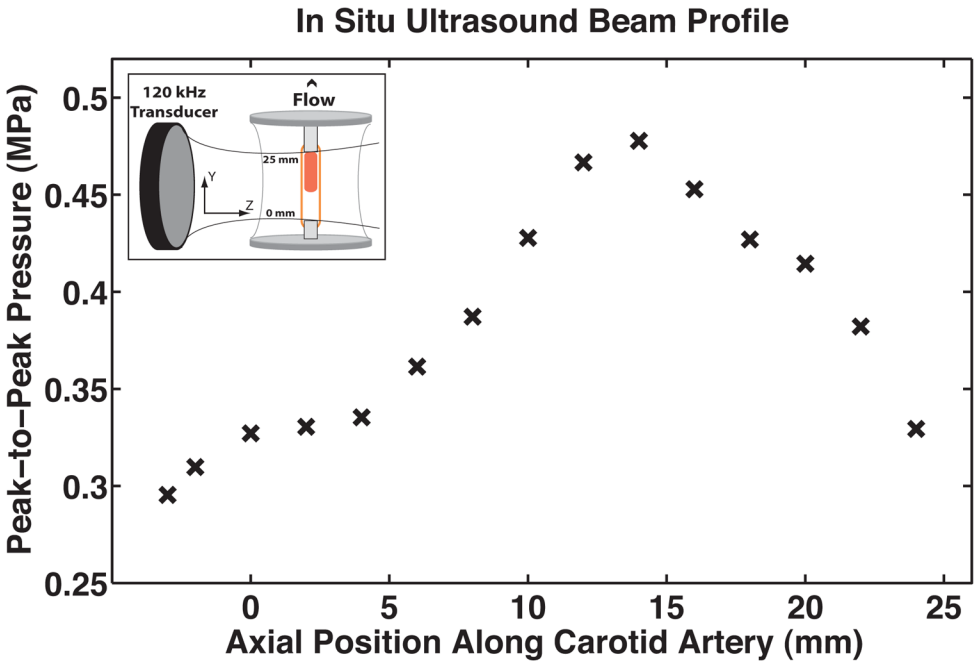

Figure 4.

The acoustic pressure profile along the axis of the carotid artery determined by an *in situ* pressure calibration using a broadband hydrophone. The peak-to-peak acoustic pressure at the axial center of the thrombus (inset) was 0.48 MPa, diminishing to roughly 0.34 MPa at the upstream and downstream faces of the thrombus. Porcine plasma flows in the positive direction.

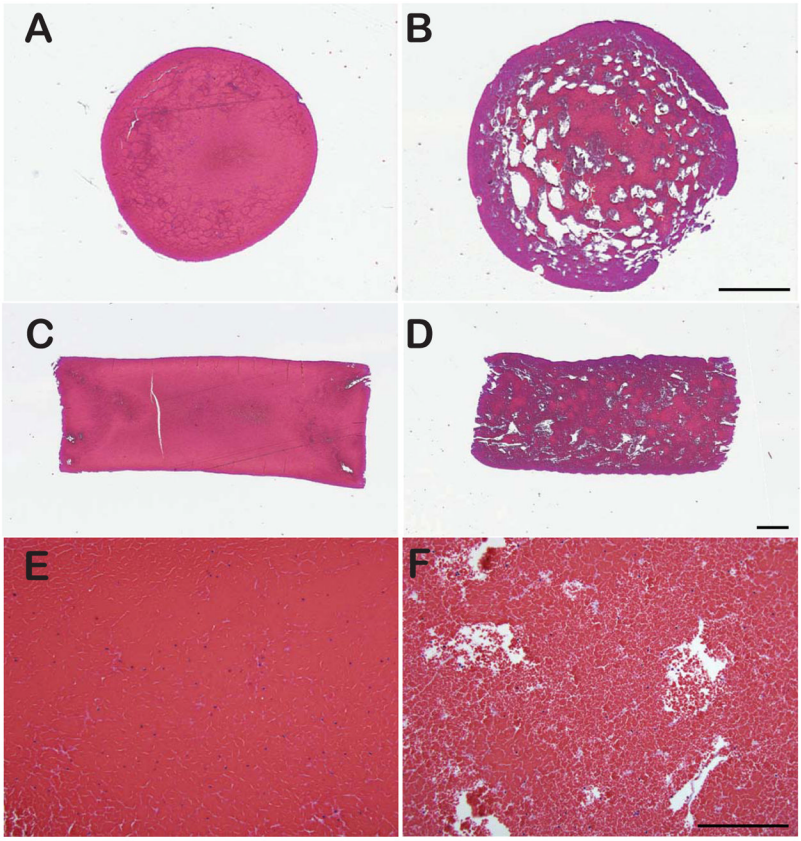

Figure 5.

Representative images of retracted (left column) and unretracted thrombi (right column) showing a cross-section (A, B), a longitudinal section (C, D) and high power 20x magnification. Stain: H&E. Bar = 1 mm in A–D, 200 μm in E–F. At 20X magnification, unretracted thrombi (B) appear much more porous than retracted thrombi (E), as evidenced by the extent of space devoid of erythrocytes and fibrin. Image analysis of these images revealed that retracted thrombi contained 0.87 ± 0.95% of this space compared to 3.45 ± 2.17% within unretracted thrombi.

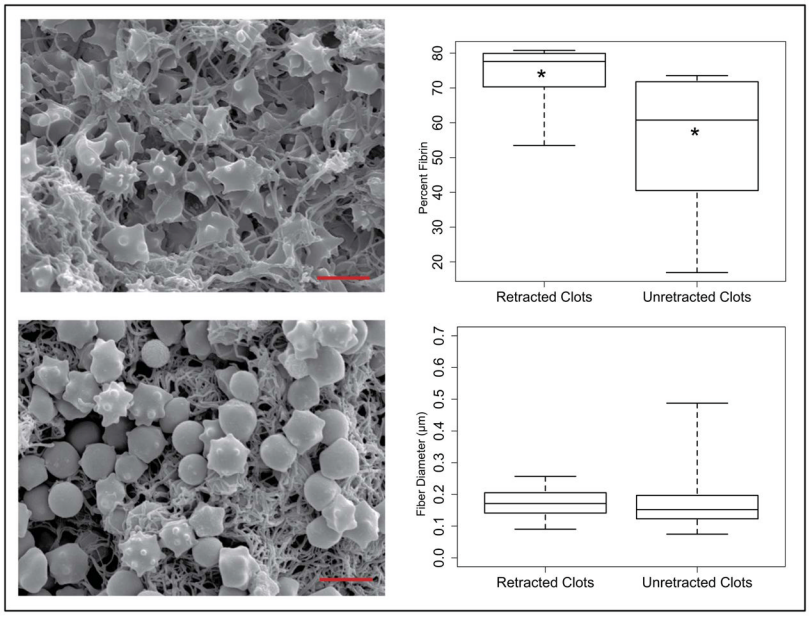

Figure 6.

Scanning electron microscopy images of the interior of representative unretracted (top left) and retracted clots (bottom left). Box and whisker plots (right column) indicate the median, 1st and 3rd quartiles, and extrema of data collected by blinded observation of fiber diameter (top right) and erythrocyte concentration (bottom right). Asterisks indicate significant differences between data medians.

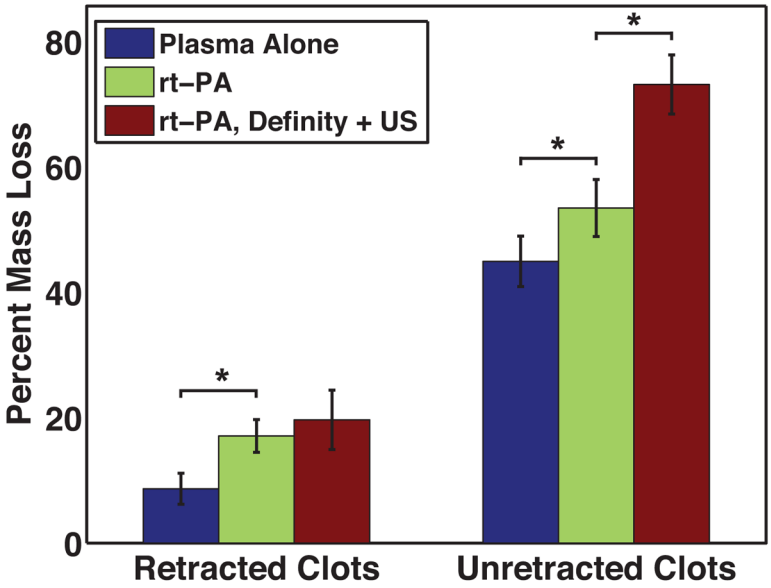

Figure 7.
Thrombolytic efficacy, as determined by percent mass loss, for plasma alone, 3.15 μg/mL rt-PA, and rt-PA, Definity + ultrasound treatments.

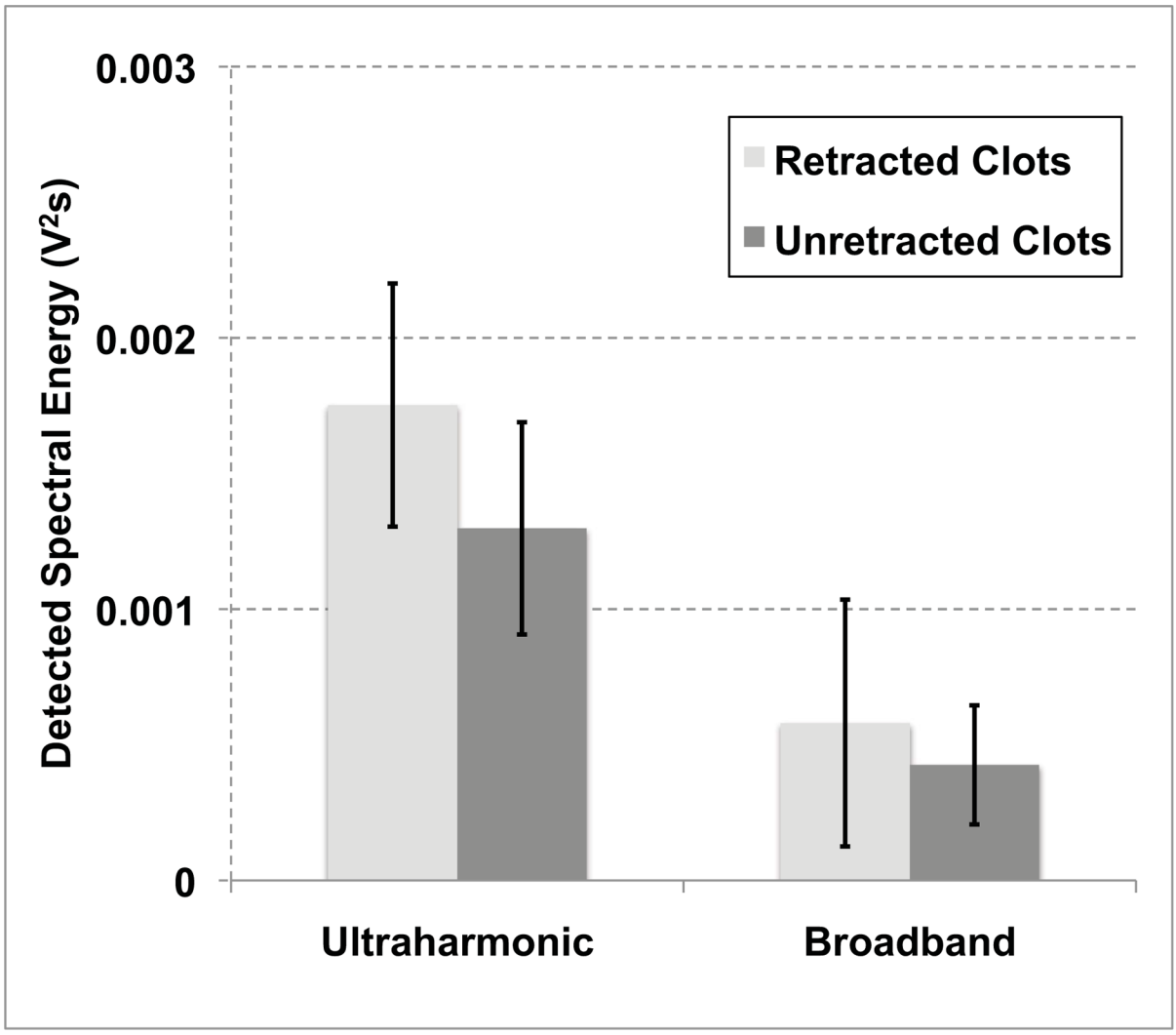

Figure 8.
The ultraharmonic and broadband energy detected by the 2.25-MHz passive cavitation detector over thirty-minute trials.

Table 1

Parameters measured in the *ex vivo* thrombosis system. Data indicate mean ± one standard deviation. Rt-PA and Definity® concentrations calculated based on the infusion pump flow rate and average flow rate through the artery.

	Plasma Alone		rt-PA		rt-PA, Definity + US	
	Retracted Clots	Unretracted Clots	Retracted Clots	Unretracted Clots	Retracted Clots	Unretracted Clots
Temperature (C)	37.53 (0.27)	36.9 (0.37)	37.09 (0.37)	37.14 (0.40)	37.23 (0.15)	37.32 (0.40)
Fluid Pressure (mmHg)	99.1 (4.0)	93.1 (6.2)	95.5 (2.5)	100.1 (4.8)	98.1 (1.5)	101.0 (4.0)
Flow Rate (mL/min)	1.54 (0.03)	1.78 (0.10)	1.40 (0.13)	1.39 (0.04)	1.46 (0.04)	1.45 (0.08)
$[\text{rt-PA}]_{calc}$ (mcg/min)	-	-	3.37 (0.24)	3.39 (0.08)	3.24 (0.08)	3.26 (0.15)
$[\text{Definity}]_{calc}$ (mcL/min)	-	-	-	-	0.29 (0.01)	0.29 (0.01)